Received: 13 July 2018 | Revised: 12 September 2018 | Accepted: 14 September 2018

DOI: 10.1002/er.4249

RESEARCH ARTICLE

WILEY INTERNATIONAL JOURNAL OF ENERGY RESEARCH

Photon management effects of hybrid nanostructures/microstructures for organic-silicon heterojunction solar cells

Yun Da[1] | Xiaojun Liu[1] | Yimin Xuan[1,2] | Qiang Li[1]

[1]School of Energy and Power Engineering, Nanjing University of Science and Technology, Nanjing 210094, China

[2]School of Energy and Power Engineering, Nanjing University of Aeronautics and Astronautics, Nanjing 210016, China

Correspondence
Yimin Xuan, School of Energy and Power Engineering, Nanjing University of Science and Technology, Nanjing 210094, China.
Email: ymxuan@mail.njust.edu.cn

Funding information
National Natural Science Foundation of China, Grant/Award Numbers: 51590901 and 51336003

Summary

Photon management and carrier separation play crucial roles on designing highly efficient organic-silicon heterojunction solar cells. Aiming at suppressing optical reflection loss and improving carrier separation efficiency simultaneously, in this paper, we experimentally fabricated hybrid nanostructured/microstructured surfaces by combining the advantages of microstructures and nanostructures. The hybrid nanostructured/microstructured surfaces were prepared by stacking nanoholes on the micropyramids via using a cost-effective method. In terms of the optical properties, the light reflection, angle-dependent light absorption, and polarization-dependent light absorption of the different structured surfaces were investigated. The results indicated that the hybrid nanostructures/microstructures exhibited ultralow reflection in the broadband wavelength range of 300 to 1100 nm (average reflection is 1.8%). Meanwhile, the hybrid nanostructured/microstructured surfaces possessed superior omnidirectional and polarization-independent properties compared to the unitary structures such as pyramid and nanohole. Furthermore, these different structured surfaces were simply used to fabricate the PEDOT:PSS/n-Si heterojunction solar cells to show the electrical properties. It was found that the PEDOT:PSS/hybrid Si solar cells showed a PCE of 9.96%, which was greater than the PEDOT:PSS/pyramid Si and PEDOT:PSS/black Si solar cells, owing to the compromise among light absorption, junction area, and minority carrier lifetime. The present work will provide a promising way to fabricate high-performance and low-cost PEDOT:PSS/n-Si heterojunction solar cells by using hybrid nanostructured/microstructured surfaces.

KEYWORDS

hybrid structured surface, omnidirectional, PEDOT:PSS/n-Si solar cells, photon management, polarization-independent

1 | INTRODUCTION

Photovoltaic cell, a pollution-free green energy resource, is considered as a promising way to mitigate the energy crisis and environmental pollution. Presently, silicon-based solar cells, which occupy over 90% market share, are the mainstream products in the commercial photovoltaic market owing to their nontoxicity, material abundance, high

reliability, acceptable efficiency, long-term stability, and mature fabrication technologies.[1] Recently, the record efficiency of the crystalline silicon (c-Si) homojunction solar cells is 25.1% while that of heterojunction solar cells reaches to 26.6%, which are very close to the theoretical limit 29.4%.[2-5] However, these traditional silicon solar cells require complex fabrication process, and their costs are very expensive, impeding their large-scale applications at present. Dopant-free carrier selective contacts are the main development direction toward highly efficient and low-cost silicon-based solar cells owing to low thermal budget, ease of processing, and simplicity of the device architecture.[6] Organic-silicon solar cells that combine the advantages of the low-cost processing for organic conjugated polymers and excellent optoelectronic characteristics of inorganic Si have been developed to reduce the cost and maintain the high performance simultaneously. The conducting polymer named poly(3,4-ehylenedioxythiophene):poly(styrenesulfonate) (PEDOT:PSS) is widely used with n-type Si to form organic-Si heterojunction solar cells due to its optical transparency, high conductivity, and excellent thermal stability.[7,8] The typical PEDOT:PSS/n-Si heterojunction solar cells are composed of front-electrode/PEDOT:PSS/n-Si/rear-electrode, where PEDOT:PSS acts as both hole-transporting layer and surface passivation layer while n-Si acts as light-absorbing layer to generate photon-generated carriers.[9,10] The fabrication process of PEDOT:PSS/n-Si solar cells has many advantages including doping-free, vacuum-free, low-temperature (<150°C) procedure, and the potential of roll-to-roll method for large-scale industrialization.[11,12] Therefore, PEDOT:PSS/n-Si heterojunction solar cells have become a remarkable potential for future low-cost and high-efficient photovoltaic devices.

So far, great efforts have been devoted to improve the efficiency of the PEDOT:PSS/Si heterojunction solar cells. The current research is mainly focused on the interface engineering and surface modification including surface passivation,[13-16] field-effect passivation,[17,18] additive treatment of PEDOT:PSS,[19-21] and rear interfacial modifications with polymers[22,23] to improve the electrical properties of the solar cells. Although these strategies can effectively boost the power conversion efficiency (PCE) of the PEDOT:PSS/Si heterojunction solar cells, the optical reflection loss is still a crucial factor limiting the device performance.[24] In order to suppress light reflection loss, photon management by using nanostructured or microstructured surface has become a common approach to be widely adopted in solar cells. There are various structured surfaces that have been proposed to enhance light absorption in PEDOT:PSS/n-Si heterojunction solar cells including cone-shaped nanohole,[25] nanocone,[26,27] nanotubes,[28] nanowires,[29,30] nanopillars,[31] pyramids,[32,33] and quasi-inverted pyramids.[34] Subramani et al combined nanotip structured surfaces and nanocrystalline silicon quantum dots to enhance the photovoltaic effects in PEDOT:PSS/Si hybrid solar cells.[35] Shen et al proposed nanowire structured surfaces to fabricate PEDOT:PSS/SiNW hybrid solar cells by improving light harvesting and enlarging contact area between the silicon substrate and polymer.[36] Yang et al investigated the contact properties of PEDOT:PSS/Si heterojunction solar cells with pyramid-textured surfaces via simulations and experiments.[37] However, all these structures belong to the unitary structures and the optical absorption of these structured surfaces is still unsatisfactory. So there is much room to improve light absorption in PEDOT:PSS/n-Si heterojunction solar cells. In addition, the angle-dependent and polarization-dependent properties of these structures are lacking as well, which play an important role in generating electricity during the day for the solar cells. Because it is known that sunlight is nonpolarized and the angle of the incidence is varied during the entire day. Thus, the solar cells with better omnidirectional and polarization-independent light absorption ability can produce more electrical energy during the day as expected. Consequently, it is of great significance to develop a functional surface with omnidirectional and polarization-independent properties for PEDOT:PSS/n-Si heterojunction solar cells.

For most existing studies, either the optical or electrical properties are separately considered. In fact, these two factors are extremely vital for high-performance solar cells. For nanostructures, despite of the ultralow optical reflection, the serious electrical recombination restricts the high efficiency of the PEDOT:PSS/n-Si heterojunction solar cells. For microstructures, although the electrical recombination can be effectively reduced, the light absorption is unsatisfactory and needs to be improved. With respect to both photon management and electrical carrier separation, a concept of hybrid structures combining the small (nanoscale) and large (microscale) structures together is expected to achieve the optimal photoelectrical properties. Wei et al proposed hierarchical structures consisting of micropyramids and nanowires to improve efficiency of Si/PEDOT:PSS solar cells.[38] Singh et al systematically investigated the optoelectronic properties of PEDOT:PSS/Si solar cells by using hierarchical structures consisting of nanostructures made over microtextured pyramidal silicon surface.[39] In their papers, they both emphasized the outstanding omnidirectional operation ability of the hierarchical Si surfaces in common, but the polarization-dependent properties of the structured surface were still lacking. Besides, the optical absorption characteristics of the hierarchical Si surfaces were still required to be improved. The challenge

of designing hybrid structures lies on how to manage light and modulate electron synergistically for the sake of realizing the optimal photoelectrical performance.

In this work, being motivated by the multiscale configuration concept, we aim to improve the photon absorption and carrier separation efficiency simultaneously by using hybrid structures. The hybrid nanostructures/microstructures consisting of nanoholes stacking over micropyramids were fabricated on the Si substrate by using anisotropic wet etching and metal-assistant chemical etching (MACE). To form hybrid nanostructures/microstructures, the micropyramid structures were prepared by using anisotropic wet etching with a mixed solution of potassium hydroxide (KOH) and flocking additive firstly. Subsequently, the nanohole structures were fabricated on the prepared micropyramid structured Si sample by using the two-step MACE technique. The advantages of the optical and electrical properties for hybrid nanostructures/microstructures were discussed separately. For photon management, the optical properties of the nanostructures/microstructures were systematically investigated, focusing on the optical benefit from both varied incident angle and polarization state. In order to obtain a desirable antireflection structured surface, the effects of etching parameters on the surface morphology and optical reflection properties were investigated to determine the optimal structured surface. The optical reflection features of different textured surfaces including planar, pyramid, black silicon nanoholes, and hybrid nanostructures/microstructures were compared to elucidate the light-trapping superiority of the hybrid structures to unitary structures. Besides, the angle-dependent and polarization-dependent properties of these different structured surfaces were analyzed. Furthermore, in terms of electrical properties, these different structured surfaces were simply used to fabricate the PEDOT:PSS/n-Si heterojunction solar cells. The current density-voltage (J-V) characteristics of different structured surfaces under AM1.5G illumination and dark conditions were analyzed. Meanwhile, the reasons behind the enhanced electrical properties of hybrid nanostructured/microstructured surfaces were revealed.

2 | EXPERIMENTAL SECTION

2.1 | Nanostructured/microstructured surface fabrication

N-type solar-grade Czochralski (CZ) Si wafers (180-μm thickness, 1-7 Ω cm, resistivity, <100> orientation) with diamond wire sawn (DWS) process were used in this experiment. Firstly, the Si wafers were cleaved into 3 cm × 3 cm square pieces, and then, these samples were ultrasonically cleaned with acetone, ethanol, and deionized (DI) water for 10 minutes, respectively. Subsequently, these pretreated samples were dried by nitrogen (N_2) for the next preparation.

Figure 1 schematically illustrates the process steps to fabricate the nanostructured/microstructured surfaces. We fabricated three types of structured surfaces including micropyramid, black Si nanohole, and hybrid nanostructures/microstructures. To fabricate the black Si random nanohole structures, a two-step MACE method was adopted.[40] On the first step, the planar Si wafers were immersed in a mixed solution of 4 mM silver nitrate ($AgNO_3$) and 0.5 vol% hydrofluoric acid (HF) for 90 seconds at room temperature to make the silver nanoparticles (AgNPs) deposited on the Si substrate. Then, it was transferred into a mixed solution composed of 12.5 vol% HF, 3 vol% hydrogen peroxide (H_2O_2), and DI water for 20 seconds at room temperature to form random nanoholes. It was noteworthy that the

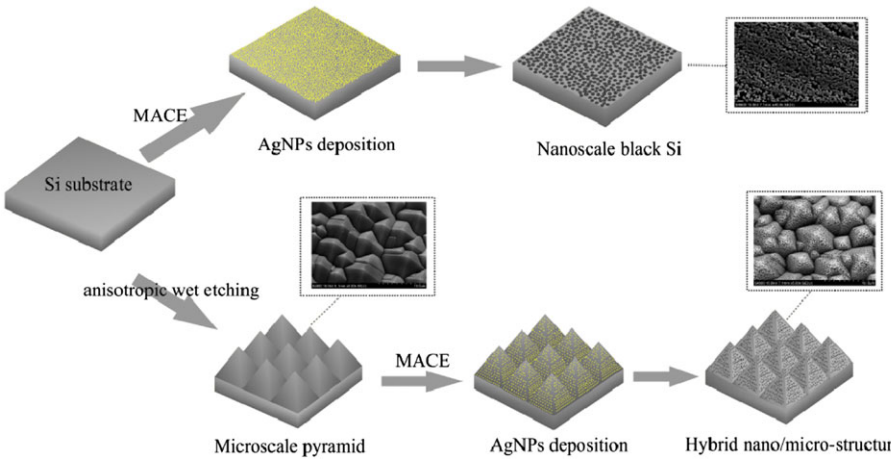

FIGURE 1 Schematic illustration for the fabrication process of the nanoblack Si structures, micropyramid structures, and hybrid nanostructures/microstructures [Colour figure can be viewed at wileyonlinelibrary.com]

concentration of $AgNO_3$ could modulate the size of the nanoholes during the AgNP deposition process. After the end of the etching, the AgNPs were removed by dipping the etched samples into concentrated nitric acid (HNO_3) and DI water for 3 minutes, respectively. It was known that metal contamination was detrimental to electrical properties of solar cells. In order to guarantee dislodging the AgNPs completely, the whole rinsing process was repeated three times. To obtain the random micropyramid structures, anisotropic wet etching method was widely used in the industry. The upside random micropyramid structures were easily shaped when the planar Si wafers were immersing into a mixed solution of 3.1 wt% KOH and 1 vol% flocking additive at a temperature of 84°C for 10 minutes. To form the hybrid nanostructured/microstructured surface, the random micropyramid structured surface was etched on the first step, followed by MACE technique to decorate the pyramid with dense nanoholes. Thus, we merely substituted the planar Si wafers into micropyramid structured wafers in the process of fabricating the black Si random nanoholes to fabricate the hybrid nanostructures/microstructures.

2.2 | Organic-silicon heterojunction solar cell fabrication

Si wafers with different structured surfaces were cut into 1.5 cm × 1.5 cm square pieces to fabricate PEDOT:PSS/n-Si heterojunction solar cells.[41] Firstly, these samples were immersed into the dilute HF solution (volume ratio: $HF/H_2O = 1:3$) for 3 minutes to remove the native Si oxide and then cleaned by DI water and dried by N_2. Subsequently, these samples were floated in a mixture of HF and HNO_3 (volume ratio: $HF/HNO_3 = 1:20$) for 5 minutes to polish the back structures. Then, these pretreated samples were cleaned up once again for the next step. Next, the PEDOT:PSS (Clevios PH 1000) solution mixed with 5 wt% dimethyl sulfoxide (DMSO) and 1 wt% Triton (Sigma-Aldrich) was deposited on the structured Si samples by spin-coating method (3600 rpm, 60 seconds) and annealed at a temperature of 120°C for 10 minutes in N_2 atmosphere. The [6,6]-phenyl-C61-butyric acid methyl ester (PCBM) precursor solution dissolved in chlorobenzene with concentration of 10 mg/mL was spin-coated on the rear side of the samples at 3000 rpm for 40 seconds without thermal annealing. Finally, 200-nm-thick Ag grid electrodes were deposited on the front side of the structured Si samples through a shadow mask while 200-nm-thick Al electrodes were deposited on the rear side by vacuum thermal evaporation (Kurt J. Lesker Mini-SPECTROS). It should be noted that the role of insertion PCBM between Si and Al was to enhance the interfacial contact quality. Besides, the PCBM layer can act as electron-selective contacts as well as surface passivation layer. The details of PCBM effects can be found in the reference of Sun's work.[41]

2.3 | Sample characterization

The surface morphologies of different structured samples were observed from field-emitting scanning electron microscopy (SEM, S-4800, Hitachi, Japan). The optical properties including reflection and transmission were measured by using a UV-Vis-NIR spectrometer (Cary 5000, Agilent Technologies Australia Pty Ltd.) with an integrating sphere in the wavelength range from 300 to 1100 nm. This spectrometer was also used to measure the optical absorption (1-R-T, R was reflection and T was transmission) at a varied incident angle of 0° to 60° for TE, TM, and unpolarized light. During the measurements of polarization state effects, the polarizer was added on the export of the incident light. In the optical measurements, the sample area was 3 cm × 3 cm. The solar simulator (Newport 91160, AM1.5G, 100 mW/cm^2) was adopted to measure the J-V characteristics under standard test conditions. In the electrical measurements, the device active area was defined by using an opaque mask with a square hole. The active area of the solar cell was fixed as 0.5 cm^2 in the experiment.

3 | RESULTS AND DISCUSSION

3.1 | Optical properties

During the MACE process, the concentration of the $AgNO_3$ plays a vital role in affecting the morphology of the Si surface. It is well known that the textured surface with different morphologies possesses different optical properties. Figure 2A to D shows the SEM images of morphological evolutions for the black Si nanohole structured surface, where the concentration of $AgNO_3$ is altered at 1, 2, 3, and 4 mM, respectively. It can be evidently observed that both the position and the size of the nanoholes were randomly distributed. Meanwhile, the average size of the nanoholes gradually increased with increasing the concentration of the $AgNO_3$. When depositing the AgNPs on the Si substrate, there were two major impacts with increasing the concentration of the $AgNO_3$. On the one hand, the distribution of the AgNPs on the Si substrate tended to become more compact as the $AgNO_3$ concentration increased. On the other hand, the seed size of the AgNPs tended to become larger with increasing the concentration of the $AgNO_3$. This was the reason why the higher concentration of $AgNO_3$ generated bigger-sized nanoholes on the Si substrate during the MACE

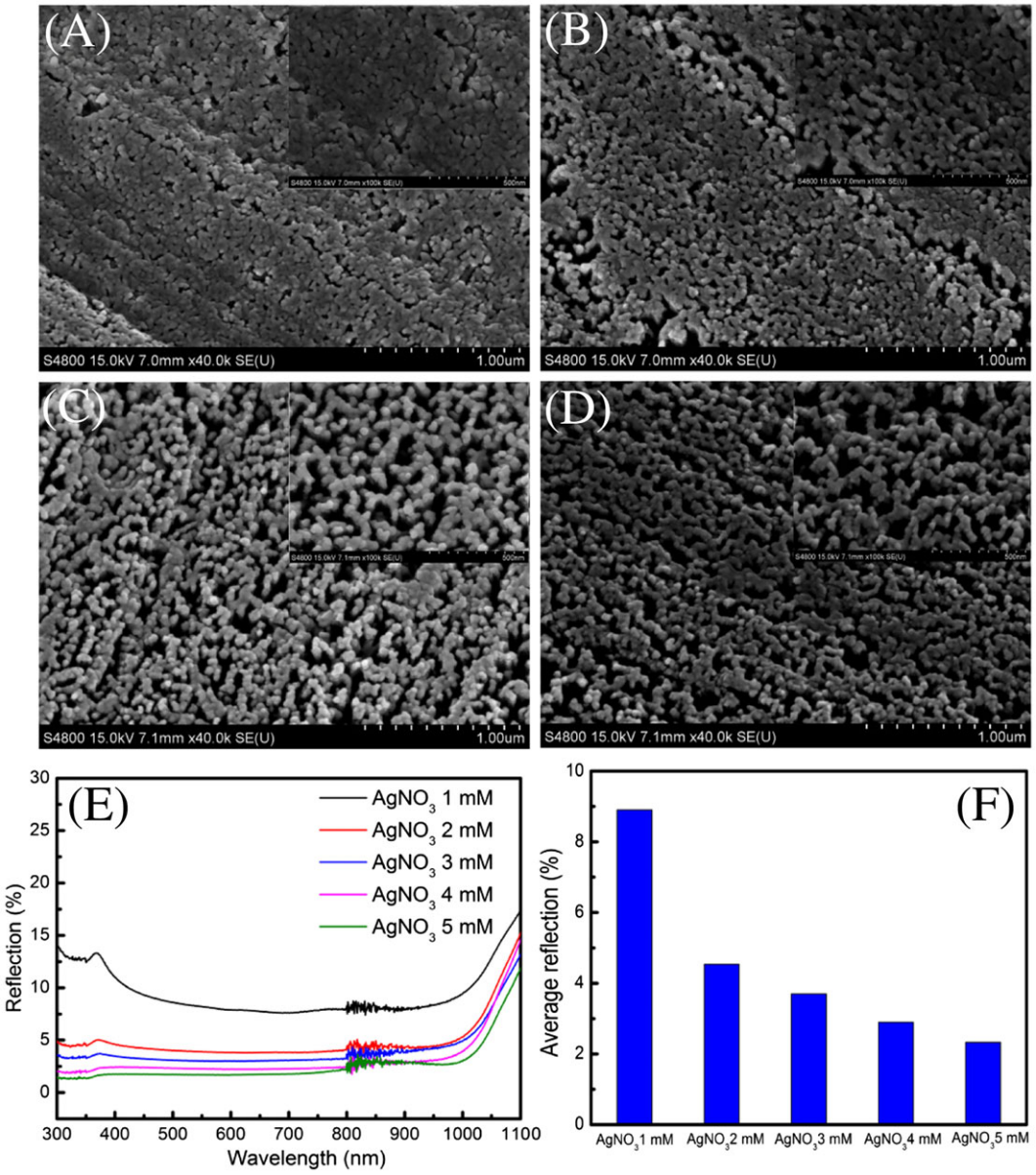

FIGURE 2 Effect of concentration of $AgNO_3$ on the black Si nanohole structured surface. A-D, Top view SEM images of the black Si nanohole surfaces with different concentration of $AgNO_3$: (A) 1 mM, (B) 2 mM, (C) 3 mM, and (D) 4 mM. E, Reflection spectra of the black Si nanohole structured surfaces under different concentrations of $AgNO_3$. F, The average reflection of the corresponding samples [Colour figure can be viewed at wileyonlinelibrary.com]

process for fabricating the black Si structured surface. Figure 2E displays the optical reflection spectrum of the random nanohole structured surfaces with various $AgNO_3$ concentrations, which were measured in the wavelength range of 300 to 1100 nm. It was obvious that the optical reflection decreased with the increment of the $AgNO_3$ concentration for black Si structured surface. When the concentration of $AgNO_3$ reached to 2 mM, the reflection is suppressed below 5% in the wavelength range from 300 to 1000 nm. If it continued to increase the concentration of $AgNO_3$, the reflection of structured surfaces became even lower, implying that the black Si nanohole structured surfaces exhibited an excellent broadband antireflective properties. Thus, the higher concentration of $AgNO_3$ can lead to lower reflection for the black Si nanohole structured surface.

In order to quantitatively evaluate the photon management ability of different textured surfaces, the average reflection and absorption were calculated by integrating the reflection and absorption with solar spectrum over the wavelength range from 300 to 1100 nm, which can be expressed as follows[42]:

$$R_{ave} = \frac{\int_{300\ \mathrm{nm}}^{1100\ \mathrm{nm}} R(\lambda) I(\lambda) d\lambda}{\int_{300\ \mathrm{nm}}^{1100\ \mathrm{nm}} I(\lambda) d\lambda} \quad (1)$$

$$A_{ave} = \frac{\int_{300\ nm}^{1100\ nm} A(\lambda)I(\lambda)d\lambda}{\int_{300\ nm}^{1100\ nm} I(\lambda)d\lambda} \quad (2)$$

where $R(\lambda)$ denotes to the reflection, $A(\lambda)$ denotes to the absorption, and $I(\lambda)$ denotes to the solar spectrum under AM1.5G illumination conditions. Figure 2F shows the average reflection of the black Si structures under different concentrations of the $AgNO_3$. As shown in Figure 2 F, the value of average reflection for black Si structured surface with $AgNO_3$ concentration of 1, 2, 3, 4, and 5 mM was 8.9%, 4.5%, 3.7%, 2.9%, and 2.3%, respectively. Obviously, in well agreement with the reflection spectrum, the black Si nanohole structured surfaces with concentration of the $AgNO_3$ at 5 mM possessed the optimal optical characteristics in suppressing the optical reflection.

Figure 3A to D shows the effects of $AgNO_3$ concentration on the morphological evolutions for the hybrid nanostructured/microstructured surface. As seen in Figure 3A to D, it was clearly found that the nanoholes can be successfully transferred onto the micropyramid structures to form hybrid nanostructures/microstructures. Similar to the black Si structures, the average size of the nanoholes in hybrid nanostructures/microstructures gradually increased with the increment of the $AgNO_3$

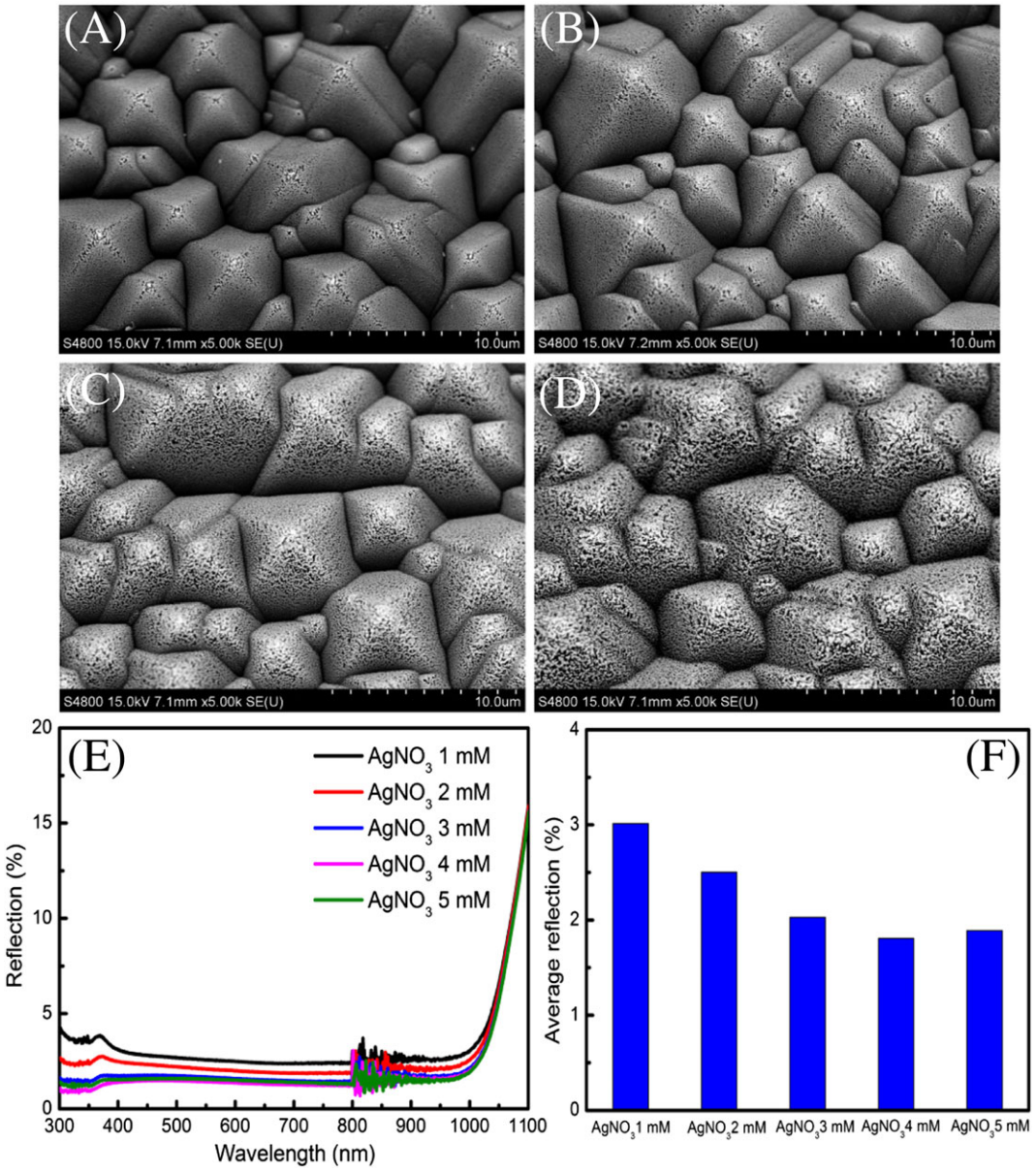

FIGURE 3 Effect of concentration of the $AgNO_3$ on the hybrid nanostructured/microstructured surface. A-D, Top view SEM images of the hybrid nanostructured/microstructured surfaces with different concentration of $AgNO_3$: (A) 1 mM, (B) 2 mM, (C) 3 mM, and (D) 4 mM. E, Reflection spectra of the hybrid nanostructured/microstructured surfaces under different concentration of $AgNO_3$. F, The average reflection of the corresponding samples [Colour figure can be viewed at wileyonlinelibrary.com]

concentration. The higher the concentration of $AgNO_3$, the rougher surfaces of the hybrid nanostructures/microstructures looked like. The reflection spectra of the hybrid nanostructured/microstructured surface with different $AgNO_3$ concentrations were shown in Figure 3E. The reflection was suppressed below 5% in the wavelength range of 300 to 1000 nm for all hybrid nanostructures/microstructures, indicating that the hybrid nanostructured/microstructured surfaces possessed superiority in light absorption. In distinction from black Si structured surfaces, the reflection spectrum increased initially and then decreased for hybrid nanostructured/microstructured surfaces with the increment of the $AgNO_3$ concentration in the range of 1 to 5 mM. Figure 3F shows the average reflection of the hybrid nanostructured/microstructured surface under different concentrations of the $AgNO_3$. The average reflection was decreased from 3.0% to 1.8% when changing the $AgNO_3$ concentration from 1 to 4 mM. When the concentration of $AgNO_3$ was further increased from 4 to 5 mM, the average reflection was increased from 1.8% to 1.9%. Obviously, the hybrid nanostructured/microstructured surface fabricated by using $AgNO_3$ concentration at 4 mM possessed the optimal optical antireflective properties. Because this work mainly focused on the superiority of the hybrid nanostructured/microstructured surfaces, the concentration of $AgNO_3$ achieved for the optimal optical antireflective properties of hybrid nanostructured/microstructured surface was preferred. Therefore, we selected the concentration of $AgNO_3$ at 4 mM to fabricate the textured surfaces in PEDOT:PSS/n-Si heterojunction solar cells.

In order to compare the light-trapping ability of unitary structures with hybrid structures, we thoroughly investigated the optical reflection properties of planar, micropyramid, nanohole black Si, and hybrid nanostructured/microstructured surface, as shown in Figure 4. Figure 4A shows the photograph of the samples with planar, pyramid, black Si, and hybrid structured surfaces and their corresponding SEM images of the microscopic structures. In macroscopic sight of the appearance, the darker color meant the lower optical reflection. Evidently, the hybrid nanostructured/microstructured surface exhibited the lowest optical reflection because it looked the darkest. Notably, when the white light impinged on the silicon-textured surfaces, the planar and black Si structured surfaces can reflect it back while it cannot happen for the pyramid and hybrid structured surfaces. This phenomenon indicated that the former were attributed to specular reflection while the latter were attributed to diffuse reflection. Hence, in spite of the black color of the black Si structures, the reflected white light can be seen at its surface. Compared to the black Si structures, the white light was more strongly reflected by the planar structures. However, although there was no reflected white light on the pyramid structures, the light-trapping ability of the black Si structures was superior to the pyramid structures because of their darker appearance. The detailed spectral characteristics can be discussed in the following. From the microscope view, different structured surfaces possessed completely different surface morphologies. For planar structures, there were many bumps and hollows on the grooved surface due to cutting damages by the DWS process. The cutting damages can be removed during the texturing process. For pyramid structures, the widths and heights were comparable at the microscale and their average sizes were estimated to be ~5 μm, as seen from cross-sectional SEM image in Figure 4A. For black Si structures, numerous random nanoholes were formed on the surface. These nanoholes belonged to the nanoscale size, and their average depths and diameters were estimated to be ~300 and ~80 nm, respectively. For hybrid nanostructures/microstructures, they were fabricated by making the nanoholes over the micropyramids and their feature sizes were comparable to the microscale pyramid and nanoscale black Si nanoholes correspondingly. It should be worth noting that the depth of the nanoholes at the top of the pyramid was slightly deeper than that at side wall of the pyramid. Figure 4B shows the reflection spectrum of different structured surfaces. It can be obviously observed that all the textured surfaces can greatly suppress the optical reflection in the overall wavelength range of 300 to 1100 nm compared to the planar structures. The textured surfaces with pyramids, black Si, and hybrid nanostructures/microstructures can availably reduce the optical reflection loss, but their antireflective physical mechanisms were different. The antireflective properties of different structured surfaces could be attributed to a number of key factors including gradient refractive index and multiple scattering effects. For the micropyramid structures, the dominant light-trapping effects were caused by the multiple rebounds of the incident light.[43,44] When the incoming light impinged on the pyramids, the reflected light can be prevented from escaping back to the air through photon management strategy of multiple rebounds, making it a second chance to be absorbed by the Si. For the black Si nanohole structures, the dominant antireflective effects can be explained by the gradient refractive index theory.[45] The gradient refractive index can realize impedance match by improving the index discontinuity and accordingly suppress the optical reflection. When the random nanoholes were introduced on the Si surface, they can be served as an effective medium and the effective refractive index was of gradient change from air to silicon, resulting in an excellent suppression

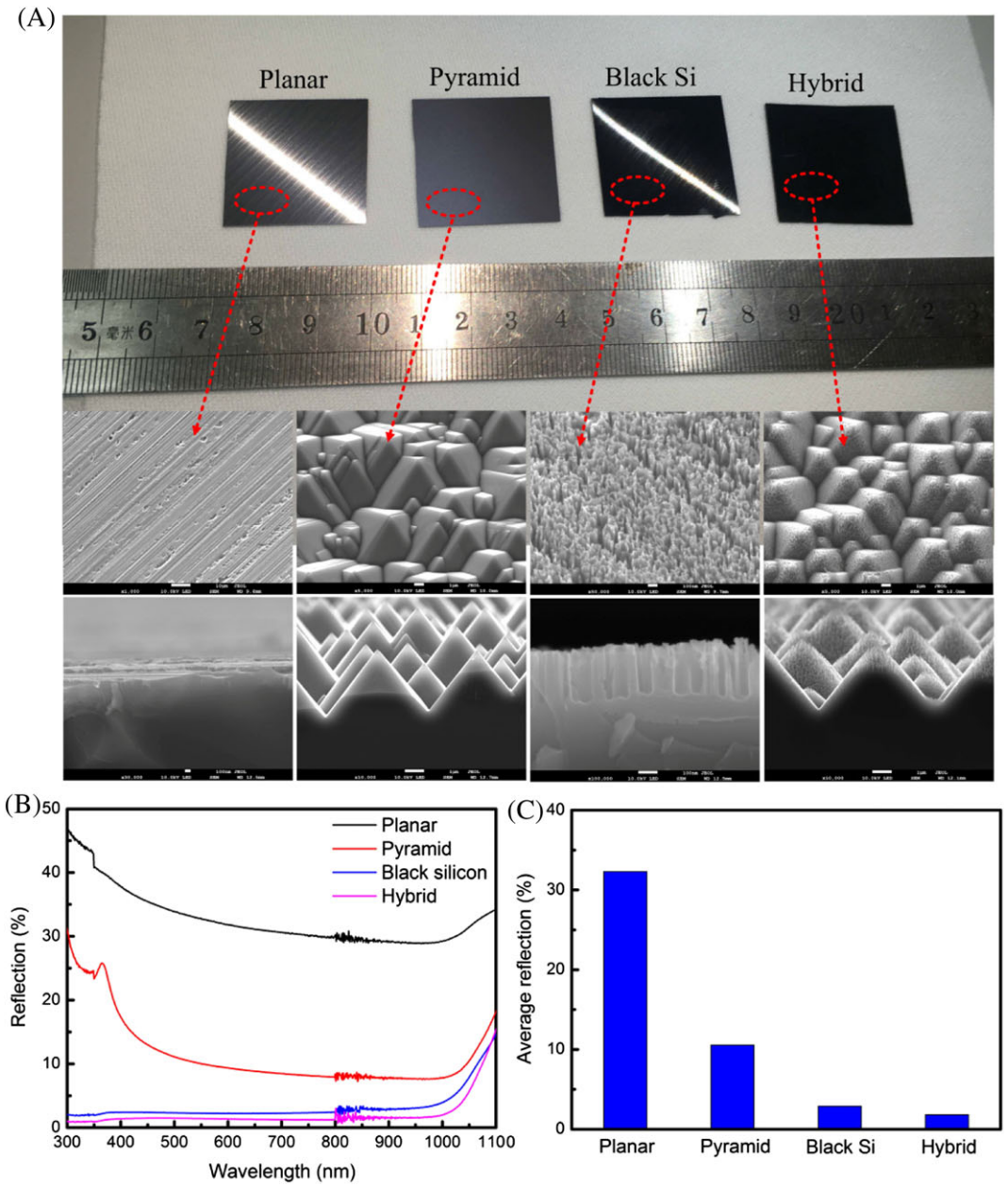

FIGURE 4 Effects of different surface textures on the optical reflection properties. A, Photograph of the samples with planar, pyramid, black Si, and hybrid structured surface. Below the photograph showing the titled and cross-sectional SEM images of the corresponding samples: (B) reflection spectra of different structured surfaces and (C) average reflection of the corresponding structured surface [Colour figure can be viewed at wileyonlinelibrary.com]

of photon reflection. For hybrid nanostructures/microstructures that combined the nanoholes with the micropyramids, they can not only realize the gradient refractive index distribution between the air and the Si surface but also allow multiple scattering effects. Thus, it was obvious that the effects induced by synergetic interaction of multiphysical mechanisms were better than that of the simplex one, resulting in lower optical reflection of hybrid nanostructures/microstructures compared to the unitary micropyramids and unitary black Si structures. Figure 4C shows the average reflection of different structured surfaces. It can be found that the average reflection of the planar surface was decreased from 32.3% to 10.6% with pyramid structured surface. The average reflection of the black Si structures was 2.9%, exhibiting superior antireflective properties compared to the pyramid structures. This result confirmed the fact of the appearance from the photograph once again. Furthermore, the average reflection of the hybrid nanostructured/microstructured surface was reduced to 1.8%, demonstrating that the hybrid nanostructures/microstructures outperformed the black Si structures.

Therefore, hybrid nanostructured/microstructured surfaces by stacking nanoholes on the pyramids exhibited superior light-trapping ability in comparison with the unitary structured surfaces.

For a high-performance photovoltaic device, the light absorption of the solar cells should be insensitive to both the incident angle and polarization state. Figure 5 shows the angle-dependent absorption spectrum of different textured surfaces for unpolarized light. The absorption spectrum of pyramid, black Si, and hybrid structures at a variable incident angle from 0° to 60° was measured to evaluate the angle dependence of the structured surfaces. As shown in Figure 5A to C, the spectral absorption was decreased as the incident angle increased for all the textured surfaces. When the incident angle changes from 0° to 60°, the variations of the spectral absorption for different structured surfaces were ranked as follows: The pyramid structure was the largest, the black Si structure took second place, and the hybrid nanostructure/microstructure was the smallest. Moreover, the tendency of the average absorption with different structured surface was consistent with the spectral absorption, as shown in Figure 5D. Obviously, the average absorption strongly depended on the incident angle for pyramid structured surface. For black Si structured surface, the angle dependence of the average absorption was not significant when the angle of the incident light was below 40°. Once the incident angle exceeded 40°, the average absorption of the black Si structure was dramatically reduced. For the hybrid nanostructured/microstructured surface, the angle dependence of the average absorption cannot be observed evidently when the incident angle varied from 0° to 60°. The reasons behind these phenomena can be attributed to the nature of the interaction between light and mater. Anyhow, these results indicated that the hybrid nanostructures/microstructures were less dependent on the incident angle than pyramid structures or black Si structures, demonstrating that the hybrid nanostructured/microstructured surface can maintain satisfactory light absorption in a wide angle.

Figure 6 shows the polarization-dependent absorption spectrum of different textured surfaces with incident angle at 0°, 30°, and 60° for TE or TM polarized light. For pyramid structure, the difference of the spectral absorption between TE and TM polarization state became more and more evident with the increment of the incident angle, as shown in Figure 6A. It can be seen from Figure 6B that the spectral absorption of the black Si structured surface exhibited a good coincidence under TE and TM polarization state as the incident angle varied

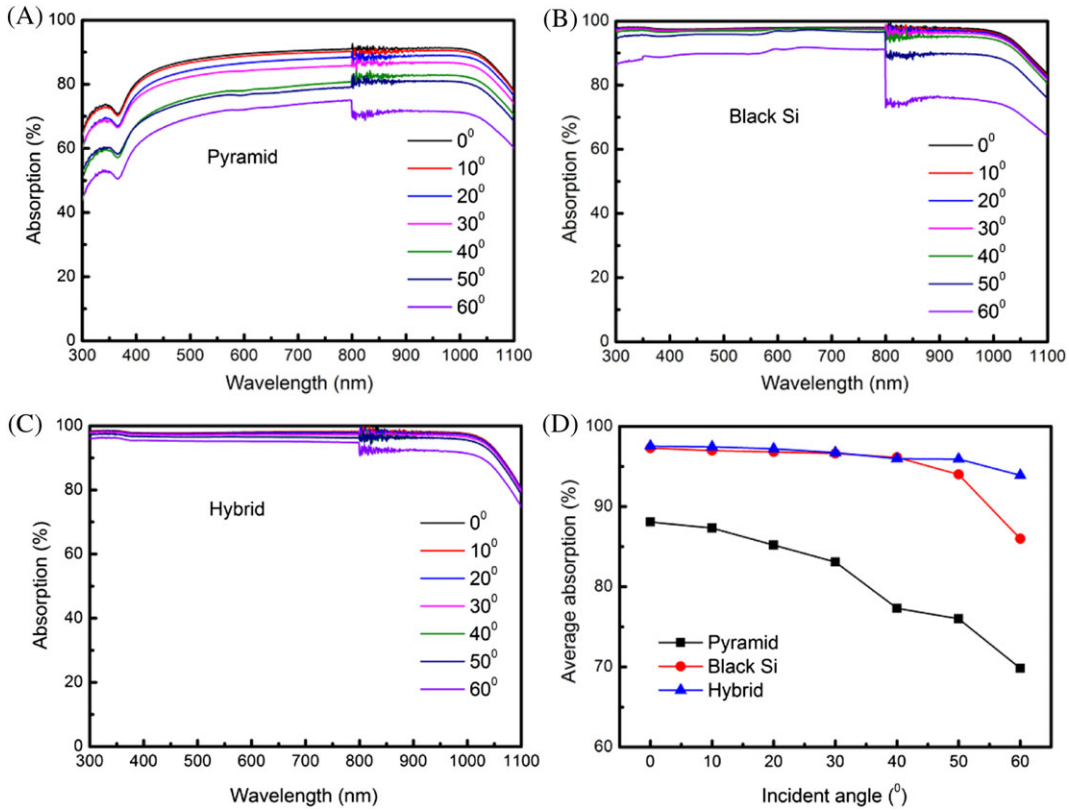

FIGURE 5 Angle-dependent spectral absorption of textured surfaces for unpolarized light. (A) Pyramid structures, (B) black Si structures, (C) hybrid nanostructures/microstructures, and (D) comparison of angle-dependent average absorption with different structured surface [Colour figure can be viewed at wileyonlinelibrary.com]

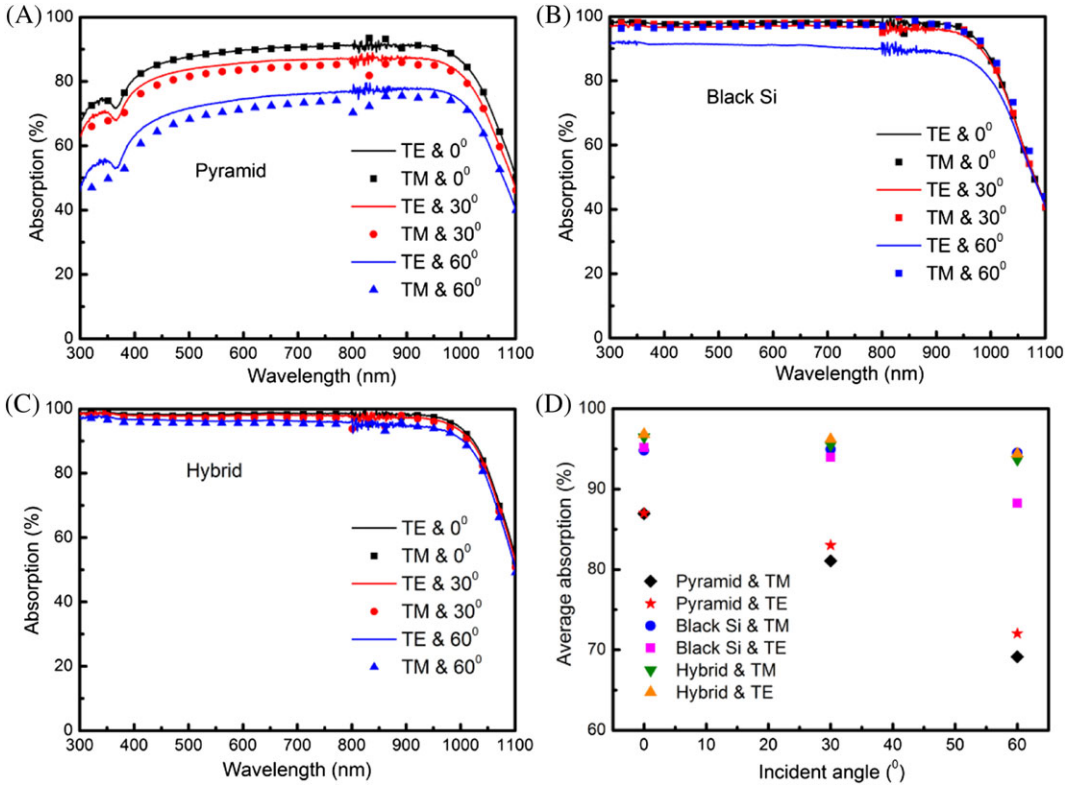

FIGURE 6 Polarization-dependent spectral absorption of different textured surface with incident angle at 0°, 30°, and 60° for TE or TM polarized light. (A) Pyramid structures, (B) black Si structures, (C) hybrid nanostructures/microstructures, and (D) comparison of polarization-dependent average absorption under distinct incident angle with different structured surface [Colour figure can be viewed at wileyonlinelibrary.com]

from 0° to 30°. However, once the incident angle was increased to 60°, very significant difference of the spectral absorption between TE and TM polarization state can be found for the black Si structured surface. For the hybrid nanostructured/microstructured surface, the spectral absorption almost coincided under TE and TM polarization state for the same incident angle, which can be seen in Figure 6C. In order to further illustrate the relationship between polarization state and incident angle quantitatively, the average absorption of different textured surfaces was calculated, as shown in Figure 6D. Apparently, the trend of the average absorption was in well agreement with the absorption spectra. As the incident angle increased, the average absorption of the hybrid nanostructured/microstructured surface was almost coincident while that of the pyramid or black Si structured surface was able to be easily distinguished under TE and TM polarization state conditions. These results indicated that the polarization state had a lowest impact on the light absorption of the hybrid nanostructured/

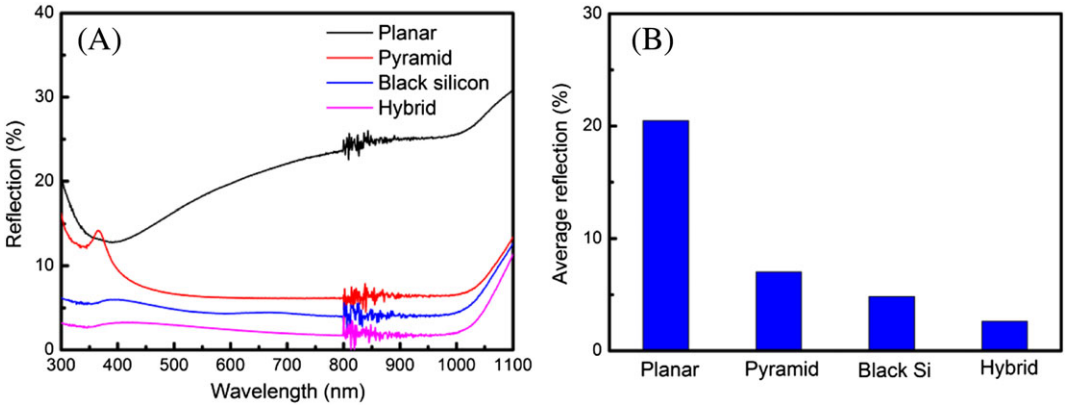

FIGURE 7 The reflection properties of the PEDOT:PSS/structured Si systems. A, Reflection spectrum. B, Average reflection [Colour figure can be viewed at wileyonlinelibrary.com]

microstructured surface compared to the pyramid and black Si structured surface. Therefore, in terms of the impacts of the incident angle and polarization state on different textured surfaces, the nanostructured/microstructured surface possessed the best omnidirectional and polarization-independent properties due to synergetic interaction of multiphysical mechanisms.

The textured silicon surface coated with PEDOT:PSS layer was the basic factor for organic-silicon heterojunction solar cells. Thus, it was meaningful to consider the spectral reflection of PEDOT:PSS/structured-Si systems. As shown in Figure 7, the spectral reflection properties of the structured silicon surfaces covered with PEDOT:PSS were similar to the structured silicon surfaces without PEDOT:PSS layer. When the planar and pyramid surfaces were covered with PEDOT:PSS layer, the average reflection was slightly decreased compared with that coated without PEDOT:PSS layer. The average reflection was reduced from 32.3% to 20.5% and 10.6% to 7.0% for planar and pyramid structured surfaces, respectively. However, for the black Si nanohole and hybrid nanostructured/microstructured surfaces, the average reflection was slight increased when covering the structured surfaces with PEDOT:PSS layer. The average reflection was decreased from 2.9% to 4.8% and 1.8% to 2.6% for black Si nanohole and hybrid nanostructured/microstructured surfaces, respectively. The reasons can be explained by gradient refractive index theory. In general, the trend of the spectral properties of the structured surfaces covered with PEDOT:PSS layer made no variance compared to the original structured surfaces.

3.2 | Electrical properties

In order to compare the electrical performance of different structured surfaces, we fabricated the PEDOT:PSS/n-Si heterojunction solar cells with these structured surfaces and measured their electrical characteristics. The current density-voltage (J-V) characteristics of the PEDOT:PSS/n-Si solar cells with different textured surfaces under AM1.5G illumination conditions were depicted in Figure 8A. The related photovoltaic parameters including short circuit current density (J_{sc}), open circuit voltage (V_{oc}), fill factor (FF), and PCE (η) are listed in Table 1. The PCE of the textured surface was sorted as follows: black Si (4.96%), pyramid (8.58%), and hybrid (9.96%). It should be noted that the PCE of the PEDOT:PSS/n-Si heterojunction solar cells with planar structures cannot be measured because of the cutting damages. Figure 9 shows the titled and cross-sectional SEM images of planar surfaces covered with PEDOT:PSS layer. As seen in Figure 9, the silicon wafers we selected had cutting damages on the surface, leading to noncontact

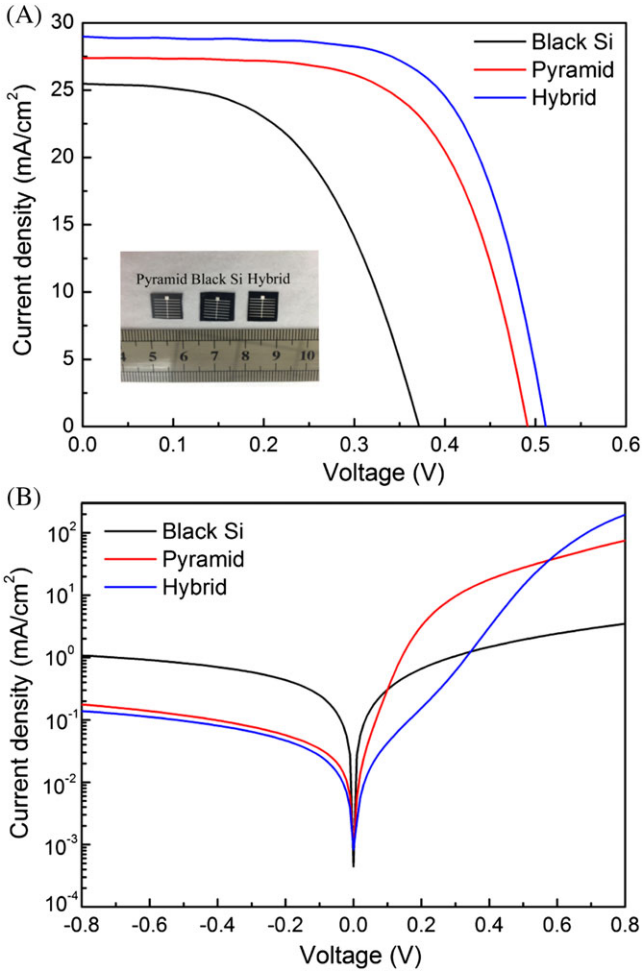

FIGURE 8 Electrical properties of pyramid, black Si, and hybrid structured surface. A, The J-V characteristics of the PEDOT:PSS/n-Si heterojunction solar cells with different structured surface under AM1.5G illumination conditions. The inset shows the photograph of the solar cells. B, The J-V characteristics of the PEDOT:PSS/n-Si solar cells in the dark conditions [Colour figure can be viewed at wileyonlinelibrary.com]

TABLE 1 Photovoltaic parameters of the PEDOT:PSS/n-Si heterojunction solar cells with different structured surfaces including pyramid, black Si, and hybrid

Textured Surface	J_{sc}, mA/cm^2	V_{oc}, mV	FF, %	η, %
Black Si	25.46	370	0.53	4.96
Pyramid	27.38	490	0.64	8.58
Hybrid	29.05	500	0.67	9.96

between planar surface and PEDOT:PSS layer in some areas. Therefore, the cutting damages at the surface made the Si and PEDOT:PSS layer form discrete contact, resulting in no measurement of PCE for PEDOT:PSS/planar-Si heterojunction solar cells. The cutting damages at the surface seriously degraded the efficiency of the PEDOT:PSS/n-Si heterojunction solar cells, and this

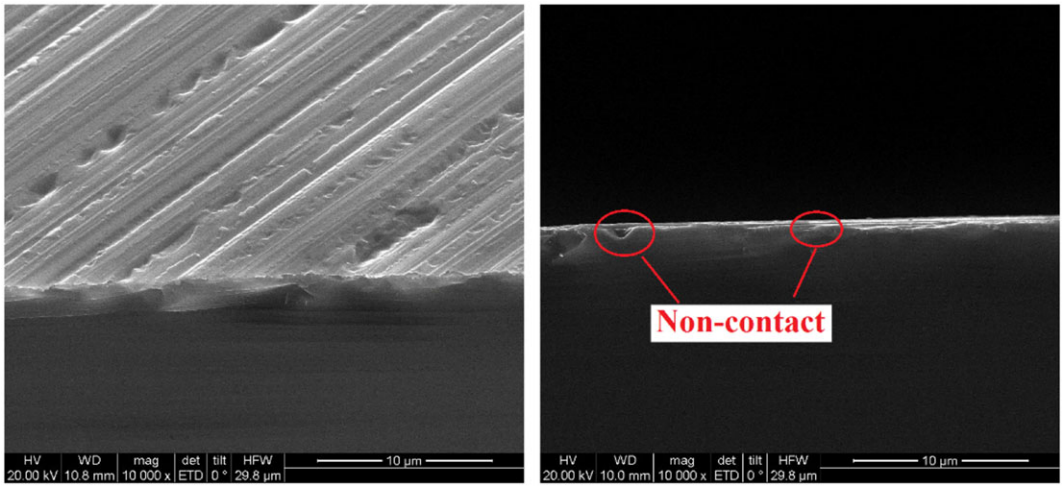

FIGURE 9 Titled and cross-sectional SEM images of planar surfaces covered with PEDOT:PSS layer [Colour figure can be viewed at wileyonlinelibrary.com]

detrimental factor should be removed in the process of fabricating the photovoltaic device. Luckily, the texturing process can remove the cutting damages. Compared to the PEDOT:PSS/pyramid-Si solar cell, the PEDOT:PSS/black-Si solar cell exhibited lower J_{sc} and η on the contrary to the optical absorption properties. Meanwhile, the *FF* of the PEDOT:PSS/black-Si solar cell was lower than the PEDOT:PSS/pyramid-Si solar cell as well. The contradiction between the lower reflection and smaller J_{sc} for black Si structured photovoltaic device compared to the pyramid one can be attributed to the carrier recombination. The direct proof was the spatial mappings of the minority carrier lifetime. As can be seen in Figure 10, the average minority carrier lifetime of the black Si structured surface coated with PEDOT:PSS layer was 4 microseconds while that of the pyramid one was 23 microseconds, which meant that the passivation of the pyramid structured surface was better than the black Si structured surface. That is to say, the recombination of black Si nanohole structured surface was more severe than that of the pyramid one, resulting in the lower V_{oc} and *FF* for black Si compared to pyramid. Using the pyramid structured surface as the reference, the PCE was boosted from 8.58% to 9.96% with the hybrid nanostructured/microstructured surface. Compared to the pyramid structured surface, the hybrid nanostructured/microstructured surface exhibited a J_{sc} of 29.05 mA/cm^2, V_{oc} of 510 mV, *FF* of 0.67, and η of 9.96%, presenting nearly 6.1% enhancement for J_{sc}, 4.1% for V_{oc}, 4.7% for *FF*, and 16.1% for η, respectively. The ameliorating effects can be attributed to the improved photon absorption and carrier separation efficiency. From the view of the minority carrier lifetime, the quality of the passivation was the highest for pyramid structured surface covered with PEDOT:PSS layer owing to the largest minority carrier lifetime. However, there were a number of impact factors determining the PCE of the solar cells including light absorption, junction area, and minority carrier lifetime. The larger junction area meant higher carrier separation efficiency. Therefore, although the carrier lifetime of the hybrid nanostructured/microstructured surface was lower than that of the pyramid one, the junction area of

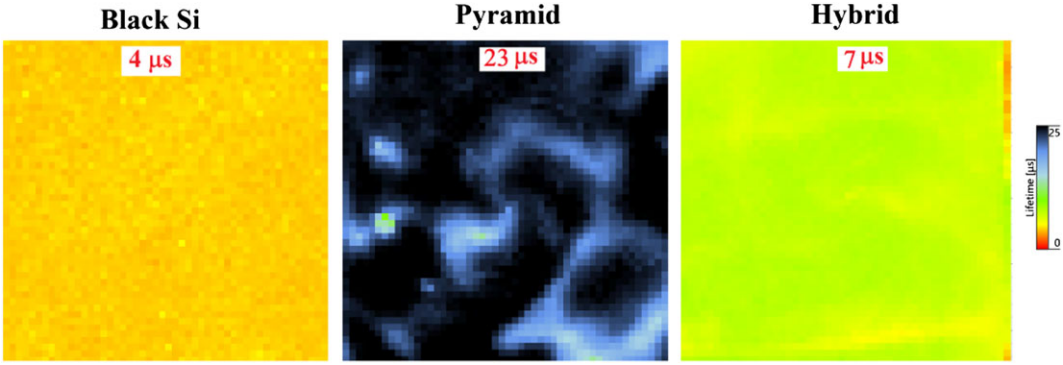

FIGURE 10 Spatial mapping of the minority carrier life for different structured surfaces covered with PEDOT:PSS layer [Colour figure can be viewed at wileyonlinelibrary.com]

the hybrid nanostructured/microstructured surface was larger than that of the pyramid one, which can be seen in Figure 11. As shown in Figure 11, the PEDOT:PSS layer suspended on the black Si structured surface, leading to no high-quality contact between Si and PEDOT:PSS layer. For pyramid structured surface, the contact between Si and PEDOT:PSS was nonconformal. But in the case of the hybrid nanostructured/microstructured surface, there seemed to be quite approaching conformal coating of PEDOT:PSS on the Si substance. These contact properties

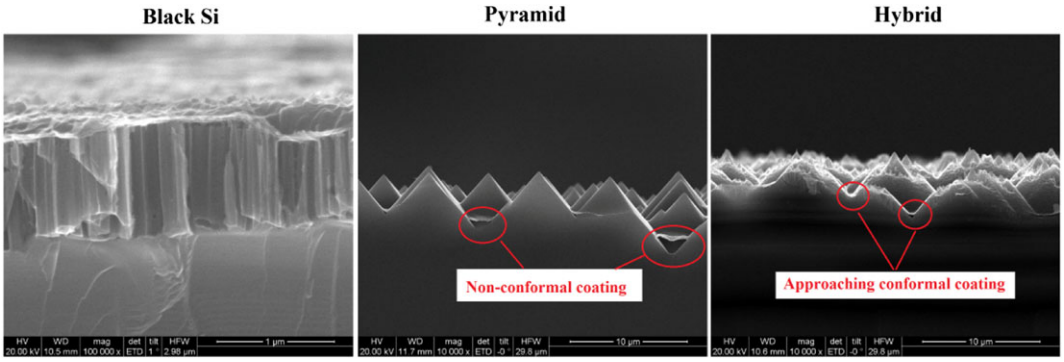

FIGURE 11 Cross-sectional SEM images of different structured surfaces with PEDOT:PSS layer [Colour figure can be viewed at wileyonlinelibrary.com]

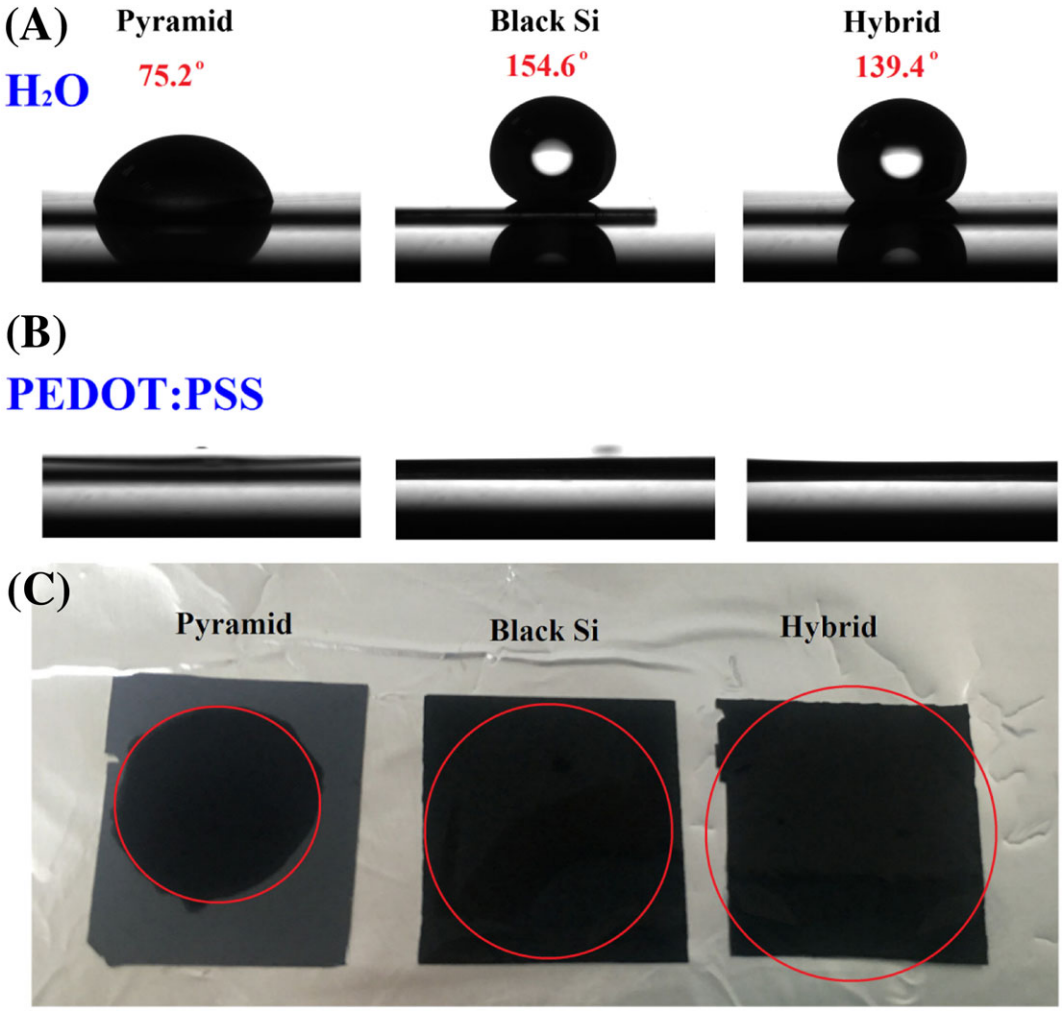

FIGURE 12 Characterization of surface wettability. A, Static contact angle measurements of water droplets. B, Static contact angle measurements of PEDOT:PSS solution droplets. C, Diffusion area of different structured surfaces with the same volume PEDOT:PSS solution droplets [Colour figure can be viewed at wileyonlinelibrary.com]

can be attributed to the distinction of surface wettability. Figure 12 shows the characterization of surface wettability for different structured surface. As seen in Figure 12 A, the static contact angle measurements of water droplets indicated that the structured surfaces exhibited hydrophobic properties, which was inconsistent with cross-sectional SEM images of different structured surfaces with PEDOT:PSS layer. However, when the water were replaced by PEDOT:PSS solution, the static contact angle measurements indicated that all the structured surfaces exhibited superhydrophilic properties, as seen in Figure 12B. Moreover, it can be observed from Figure 12C that the size of diffusion area for hybrid nanostructured/microstructured surface was the largest compared to the pyramid and black Si, indicating that the hybrid nanostructured/microstructured surface exhibited the best surface wettability. The characterization of surface wettability confirmed the fact that the hybrid nanostructured/microstructured surfaces possessed the best contact properties with PEDOT:PSS layer. As a consequence, the compromise among light absorption, minority carrier lifetime, and junction area resulted in the highest PCE of the hybrid nanostructured/microstructured photovoltaic device compared to the pyramid and black Si.

Figure 8B shows the J-V characteristics with different structured surfaces in dark conditions. It should be well known that the properties of dark current can deliver the properties of recombination in solar cells. Obviously, it can be seen from Figure 8B that the heterojunction solar cell of PEDOT:PSS/hybrid-Si possessed the smallest reversed saturation current and recombination current while PEDOT:PSS/pyramid-Si took the second, and PEDOT:PSS/black-Si had the largest. The large reversed saturation current and recombination current would lead to decrease the open circuit voltage V_{oc} and then suppress the device performance. These results indicated that recombination in PEDOT:PSS/hybrid-Si solar cells is minimal due to improved carrier separation efficiency originating from synergistic effects including surface wettabiliy, junction area, and minority carrier lifetime. Therefore, the hybrid nanostructured/microstructured surface can simultaneously achieve the optimal optical and electrical characteristics, providing a great potential for highly efficient heterojunction solar cell applications.

It should be noted that the best PCE of the PEDOT:PSS/n-Si heterojunction solar cells in this work (9.96%) is slightly lower than that reported by other research groups. Nevertheless, the PCE is closely related to many impact factors such as quality of silicon wafers (electronic grade, solar grade, metallurgical grade), doping density, thickness, surface nanostructures/microstructures, quality of PEDOT:PSS and additive, the configuration of the photovoltaic device, metal contacts (eg, Au, Ti/Au, Ag, Ti/Ag, Al, Mg/Al, Ca/Al, Sc/Al, In-Ga, or ITO/glass), fabrication process, device size, and so on. Thus, a direct comparison of PCE of different research groups is difficult and unfair. The highlight of this work is to illustrate the effects of photon management on the performance of organic-silicon heterojunction solar cells, and we have proved that it is suitable to improve the PCE of the PEDOT:PSS/n-Si heterojunction solar cells by adopting the hybrid nanostructures/microstructures. Moreover, it should be noted that the hybrid nanostructures/microstructures have a lot more potential to reach a higher PCE by selecting a higher quality silicon wafer, a better passivation process, a more suitable metal contact, an optimized fabrication process, and so on.

4 | CONCLUSIONS

In summary, we presented a cost-effective method to fabricate hybrid nanostructured/microstructured surface by combining anisotropic wet etching and MACE. The hybrid nanostructured/microstructured surface can effectively suppress the optical reflection loss in a broadband wavelength range from 300 to 1100 nm, and the average reflection was decreased to 1.8%. Meanwhile, the hybrid nanostructured/microstructured surface exhibited omnidirectional and polarization-independent properties as well, making it suitable for solar cells. Compared to the unitary structures such as planar, pyramid, and black Si, the hybrid nanostructures/microstructures were the least dependent on the incident angle and polarization state. Furthermore, in terms of the electrical properties, the PEDOT:PSS/hybrid-Si showed a PCE of 9.96%, which was greater than the PEDOT:PSS/pyramid-Si and PEDOT:PSS/black-Si solar cells, owing to the compromise among light absorption, junction area, and minority carrier lifetime. Through optical and electrical analysis, it was found that the hybrid nanostructured/microstructured surface can not only reduce optical reflection loss to achieve excellent photon management properties but also improve the carrier separation efficiency originating from synergistic effects including surface wettabiliy, junction area, and minority carrier lifetime. Consequently, our results indicated that hybrid nanostructured/microstructured surface was preferred to fabricate highly efficient PEDOT:PSS/n-Si heterojunction solar cells. Our findings of hybrid structures with omnidirectional and polarization-independent properties may provide a great potential for high-performance heterojunction solar cells applications.

ACKNOWLEDGEMENTS

The first author would like to thank Prof. Baoqun Sun from Soochow University for his providing facilities of fabricating photovoltaic devices and Mr. Peng Gao and Ms. Yujie Han from Soochow University for their supports during the experimental processes. This work is financially supported by the National Natural Science Foundation of China (Grant No. 51336003 and No. 51590901).

ORCID

Yimin Xuan http://orcid.org/0000-0002-4053-9946

REFERENCES

1. Gao P, Yang Z, He J, et al. Dopant-free and carrier-selective heterocontacts for silicon solar cells: recent advances and perspectives. *Adv Sci*. 2018;5(3):1700547.
2. Polman A, Knight M, Garnett EC, Ehrler B, Sinke WC. Photovoltaic materials: present efficiencies and future challenges. *Science*. 2016;352(6283):aad4424.
3. Yoshikawa K, Yoshida W, Irie T, et al. Exceeding conversion efficiency of 26% by heterojunction interdigitated back contact solar cell with thin film Si technology. *Sol Energy Mater Sol Cells*. 2017;173:37-42.
4. Yoshikawa K, Kawasaki H, Yoshida W, et al. Silicon heterojunction solar cell with interdigitated back contacts for a photoconversion efficiency over 26%. *Nat Energy*. 2017;2(5):17032.
5. Richter A, Hermle M, Glunz SW. Reassessment of the limiting efficiency for crystalline silicon solar cells. *IEEE J Photovolt*. 2013;3(4):1184-1191.
6. Yang Z, Gao P, Sheng J, et al. Principles of dopant-free electron-selective contacts based on tunnel oxide/low work-function metal stacks and their applications in heterojunction solar cells. *Nano Energy*. 2018;46:133-140.
7. Zhang Y, Liu R, Lee ST, Sun B. The role of a LiF layer on the performance of poly (3, 4-ethylenedioxythiophene): poly (styrenesulfonate)/Si organic-inorganic hybrid solar cells. *Appl Phys Lett*. 2014;104(8):083514.
8. Groenendadal L, Jonas F, Freitag D, Pielartzik H, Reynolds JR. Poly (3,4-ethylenedioxythiophene) and its derivatives: past, present, and future. *Adv Mater*. 2000;12(7):481-494.
9. Wu S, Cui W, Aghdassi N, et al. Nanostructured Si/organic heterojunction solar cells with high open-circuit voltage via improving junction quality. *Adv Funct Mater*. 2016;26(28):5035-5041.
10. Jackle S, Liebhaber M, Gersmann C, et al. Potential of PEDOT: PSS as a hole selective front contact for silicon heterojunction solar cells. *Sci Rep*. 2017;7(1):2170.
11. Jiang X, Zhang P, Zhang J, et al. High performance of PEDOT: PSS/n-Si solar cells based on textured surface with AgNWs electrodes. *Nanoscale Res Lett*. 2018;13(1):53.
12. Kasahara K, Hossain J, Harada D, Ichikawa K, Ishikawa R, Shirai H. Crystalline-Si heterojunction with organic thin-layer (HOT) solar cell module using poly(3,4-ethylenedioxythiophene): poly (styrene sulfonate) (PEDOT: PSS). *Sol Energy Mater Sol Cells*. 2018;181:60-70.
13. Chen J, Shen Y, Guo J, et al. Electrochemical grafting passivation of silicon via electron transfer at polymer/silicon hybrid interface. *Electrochim Acta*. 2017;247:826-834.
14. Sheng J, Fan K, Wang D, et al. Improvement of the SiO_x passivation layer for high-efficiency Si/PEDOT:PSS heterojunction solar cells. *ACS Appl Mater Interfaces*. 2014;6(18):16027-16034.
15. Yoon SS, Khang DY. High efficiency (>17%) Si-organic hybrid solar cells by simultaneous structural, electrical, and interfacial engineering via low-temperature processes. *Adv Energy Mater*. 2018;8(9):1702655.
16. Yoon SS, Lee GR, Khang DY. Contact-printed ultrathin siloxane passivation layer for high-performance Si-PEDOT:PSS hybrid solar cells. *Microelectron Eng*. 2017;170:1-7.
17. Liu Z, Yang Z, Wu S, et al. Photoinduced field-effect passivation from negative carrier accumulation for high-efficiency silicon/organic heterojunction solar cells. *ACS Nano*. 2017;11(12):12687-12695.
18. Wang Y, Xia Z, Liu L, et al. The light-induced field-effect solar cell concept—perovskite nanoparticle coating introduces polarization enhancing silicon cell efficiency. *Adv Mater*. 2017;29(18):1606370.
19. Pathak CS, Singh JP, Singh R. Effect of dimethyl sulfoxide on the electrical properties of PEDOT:PSS/n-Si heterojunction diodes. *Curr Appl Phys*. 2015;15(4):528-534.
20. Pathak CS, Singh JP, Singh R. Optimizing the electrical properties of PEDOT:PSS films by co-solvents and their application in polymer photovoltaic cells. *Appl Phys Lett*. 2017;111(10):102107.
21. Ikeda N, Koganezawa T, Kajiya D, Saitow KI. Performance of Si/PEDOT:PSS hybrid solar cell controlled by PEDOT:PSS film nanostructure. *J Phys Chem C*. 2016;120(34):19043-19048.
22. Han Y, Liu Y, Yuan J, et al. Naphthalene Diimide-based n-type polymers: efficient rear interlayers for high-performance silicon-organic heterojunction solar cells. *ACS Nano*. 2017;11(7):7215-7222.
23. He J, Zhang W, Ye J, Gao P. 16% efficient silicon/organic heterojunction solar cells using narrow band-gap conjugated polyelectrolytes based low resistance electron-selective contacts. *Nano Energy*. 2018;43:117-123.
24. Meng F, Dehouche Z, Nutasarin A, Fren GR. Effective MgO-doped TiO2 nanoaerogel coating for crystalline silicon solar cells improvement. *Int J Energy Res*. 2018;1-13.
25. Wang Z, Peng S, Wen Y, et al. High-performance Si/organic hybrid solar cells using a novel cone-shaped Si nanohole structures and back surface passivation layer. *Nano Energy*. 2017;41:519-526.
26. Jeong S, Garnett EC, Wang S, et al. Hybrid silicon nanocone-polymer solar cells. *Nano Lett*. 2012;12(6):2971-2976.
27. Wang H, Wang J. Rusli hybrid Si nanocones/PEDOT:PSS solar cell. *Nanoscale Res Lett*. 2015;10:191.

28. Jeong H, Song H, Pak Y, et al. Enhanced light absorption of silicon nanotube arrays for organic/inorganic hybrid solar cells. *Adv Mater*. 2014;26(21):3445-3450.
29. Sharma M, Pudasaini PR, Ruiz-Zepeda F, Elam D, Ayon AA. Ultrathin, flexible organic-inorganic hybrid solar cells based on silicon nanowires and PEDOT:PSS. *ACS Appl Mater Interfaces*. 2014;6(6):4356-4363.
30. Liu R, Wang J, Sun T, et al. Silicon nanowire/polymer hybrid solar cell-supercapacitor: a self-charging power unit with a total efficiency of 10.5%. *Nano Lett*. 2017;17(7):4240-4247.
31. Pudasaini PR, Ruiz-Zepeda F, Sharma M, Elam D, Ponce A, Ayon AA. High efficiency hybrid silicon nanopillar-polymer solar cells. *ACS Appl Mater Interfaces*. 2013;5(19):9620-9627.
32. He J, Gao P, Yang Z, et al. Silicon/organic hybrid solar cells with 16.2% efficiency and improved stability by formation of conformal heterojunction coating and moisture-resistant capping layer. *Adv Mater*. 2017;29(15):1606321.
33. Wang X, Liu Z, Yang Z, et al. Heterojunction hybrid solar cells by formation of conformal contacts between PEDOT:PSS and periodic silicon nanopyramid arrays. *Small*. 2018;14(15):1704493.
34. Tang Q, Shen H, Yao H, et al. Potential of quasi-inverted pyramid with both efficient light trapping and sufficient wettability for ultrathin c-Si/PEDOT:PSS hybrid solar cells. *Sol Energy Mater Sol Cells*. 2017;169:226-235.
35. Subramani T, Chen J, Sun YL, Jevasuwan W, Fukata N. High-efficiency silicon hybrid solar cells employing nanocrystalline Si quantum dots and Si nanotips for energy management. *Nano Energy*. 2017;35:154-160.
36. Shen R, Liu M, Zhou Y, et al. PEDOT:PSS/SiNWs hybrid solar cells with an effective nanocrystalline silicon back surface field layer by low temperature catalytic diffusion. *Solar RRL*. 2017;1(11):1700133.
37. Yang Z, Gao P, He J, et al. Tuning of the contact properties for high-efficiency Si/PEDOT:PSS heterojunction solar cells. *ACS Energy Lett*. 2017;2(3):556-562.
38. Wei WR, Tsai ML, Ho ST, et al. Above-11%-efficiency organic-inorganic hybrid solar cells with omnidirectional harvesting characteristics by employing hierarchical photon-trapping structures. *Nano Lett*. 2013;13(8):3658-3663.
39. Singh P, Srivastava SK, Sivaiah B, Prathap P, Rauthan CMS. Enhance photovoltaic performance of PEDOT:PSS/Si solar cells using hierarchical light trapping scheme. *Solar Energy*. 2018;170:221-233.
40. Oh J, Yuan HC, Branz HM. An 18.2%-efficient black-silicon solar cell achieved through control of carrier recombination in nanostructures. *Nat Nanotechnol*. 2012;7(11):743-748.
41. Liu J, Ji Y, Liu Y, et al. Doping-free asymmetrical silicon heterocontact achieved by integrating conjugated molecules for high efficient solar cell. *Adv Energy Mater*. 2017;7(19):1700311.
42. Huang Z, Zhong S, Hua X, et al. An effective way to simultaneous realization of excellent optical and electrical performance in large-scale Si nano/microstructures. *Prog Photovolt*. 2015;23(8):964-972.
43. Liu Y, Zi W, Liu S, Yan B. Effective light trapping by hybrid nanostructure for crystalline silicon solar cells. *Sol Energy Mater Sol Cells*. 2015;140:180-186.
44. Liu D, Wang Q, Shen W, Wang D. Self-cleaning antireflective coating with a hierarchical texture for light trapping in micromorph solar cells. *J Mater Chem C*. 2017;5(1):103-109.
45. Chang CH, Dominguez-Caballero JA, Choi HJ, Barbastathis G. Nanostructured gradient-index antireflection diffractive optics. *Opt Lett*. 2011;36(12):2354-2356.

How to cite this article: Da Y, Liu X, Xuan Y, Li Q. Photon management effects of hybrid nanostructures/microstructures for organic-silicon heterojunction solar cells. *Int J Energy Res*. 2018;1–16. https://doi.org/10.1002/er.4249